J. Indian Inst. Sci., May–June 2005, **85**, 119–129

Buoyancy-driven convection in liquid metals subjected to transverse magnetic fields

V. MITTAL[†,*], M. F. BAIG[#] AND B. KANT KHAN[#]
[†]Department of Mechanical Engineering, BRCM College of Engineering and Technology, Bahal 127 028, Haryana, India.
[#]Department of Mechanical Engineering, Aligarh Muslim University, Aligarh, UP, India.
email: vmittal1231@rediffmail.com

Received on April 2, 2004: Revised on November 3, 2004.

Abstract

This study presents the numerical simulation of Navier–Stokes, energy and hydromagnetic equations to analyse two-dimensional natural convection of liquid metals subjected to transverse magnetic field. The spatio-temporal study shows that the oscillatory flow changes to steady fluid flow pattern with increase in intensity of applied magnetic field for a range of Rayleigh number (*Ra*) between 10^5 and 10^8. The strength of magnetic field governs the pattern formation as well as the amplitude of the velocities for any particular Rayleigh number in the above range. The amplitude of aperiodic oscillations of any dynamical variable at higher *Ra* gets significantly damped out, especially removal of low-power harmonics with increase in the strength of magnetic field through variation of Chandrasekhar number.

Keywords: Natural convection, transverse magnetic field, Rayleigh number, Chandrasekhar number.

1. Introduction

It is well known that convective turbulent fluctuations can be significantly suppressed in liquid metals by the application of an external magnetic field. This phenomenon is being successfully used in solidification process to weaken the buoyancy-driven fluctuations, to modify the interface shape and the rate of solidification in the manufacturing processes of semiconductor crystals [1]. Moreover, external magnetic field also plays an important role in affecting nucleation, crystal growth, segregation, etc. by controlling the fluid flow in metallurgical processes [2]. In many energy-conversion processes, strong external magnetic fields are applied to liquid metal flows in electrically insulated ducts. For example, liquid lithium is used to extract energy from fusion reactor and to breed the tritium to fuel the fusing plasma during which liquid lithium must be pumped through strong magnetic field needed to confine the plasma [3].

Besides analytical and experimental work, the impetus has now shifted to numerical study of these problems to understand the physics involved in the interaction of magnetic field with large-scale flow structures and in analysing dynamics and kinematics of the magnetohydrodynamic flow field [4]. Such magnetoconvective flows in bounded domains have

*Author for correspondence.

been solved through two- and three-dimensional numerical simulations by several researchers in recent years. Ozoe and Maruo [5] numerically studied the two-dimensional natural convection of liquid metals with transverse magnetic field in a square enclosure. They varied the Rayleigh number (*Ra*) from 10^4 to 10^6, and the Hartmann number (*Ha*) from 1 to 10^3 for liquid silicon, and gave a correlation for Nusselt number (*Nu*). Ozoe and Okada [6] later computationally solved the three-dimensional natural convection in cubical enclosure with external magnetic field applied in either X, Y or Z directions. They found that the magnetic field parallel to the vertical hot and cold walls was the least effective in suppressing convection, while that applied transverse was the most effective.

Hadjiloucas *et al*. [7] solved numerically the two-dimensional natural convection in low *Pr* liquids for a differentially heated cavity of varying aspect ratio subjected to vertical and horizontal magnetic fields. They found that in tall cavities, under weak magnetic fields, the flow becomes oscillatory and even chaotic at high *Ra*. Alchaar *et al*. [8] numerically investigated the effect of transverse magnetic field on natural convection in a shallow rectangular cavity (horizontal Bridgeman configuration). They presented results for the temperature and velocity profiles in terms of Hartmann number and found that the velocity gradient in the core is constant outside the two Hartmann layers near the vicinity of walls normal to the magnetic field. Juel *et al*. [9] performed numerical as well as experimental work to analyse flow patterns, temperature and velocity profiles in magnetoconvection in molten gallium.

The magnetoconvection in confined domains has its dynamics entirely governed by five dimensionless parameters, namely, Rayleigh number (*Ra*), Hartmann number (*Ha*) or its square, i.e. the Chandrasekhar number (*Q*), Prandtl number (*Pr*), Magnetic Prandtl number (*Pm*) and Aspect ratio (*AR*). The aim of the present study is to analyse the interaction of buoyancy and electromagnetic forces on the development of spatio-temporal pattern formation. To realize this interaction, the strength of applied magnetic field through *Q* for a range of *Ra* has been numerically varied by solving two-dimensional Navier–Stokes, energy and magnetohydrodynamic equations for liquid metals. We have also investigated the influence of vertical side walls of unity aspect ratio enclosure on the formation of patterns as well as its effect on temporal history of dynamical variables. This has also been performed to ascertain the route of transition to spatio-temporal chaos as the controlling parameter *Ra* is increased for a fixed value of *Q*.

For this, we have used nonlinear dynamics, spectral and statistical tools to understand the dynamics of the flow. The mechanism of the special flow features found are explained and their influence on heat transfer capabilities has been investigated.

In the present study, we have fixed magnetic Reynolds number $R_m = P_m/Pr = 0.1$, $Pr = 0.015$, $P_m = 0.0015$ and varied the *Q* in the range 9 to $9*10^4$ and *Ra* from 10^5 to 10^8 to analyse spatio-temporal dynamics for a broad range of controlling parameters. The parameters cover the kinematic range where the magnetic field is sufficiently weak for the Lorentz forces to be neglected to a field that is strong enough to suppress the convection altogether. In Section 2, mathematical modelling of the governing equations and implementation of boundary conditions has been performed. A concise summary of solution methodology involved in the numerical approximation of the governing equations is also provided. Section

3 presents the results and discussion pertaining to validation of the code, variation of Q at fixed Ra and of Ra at fixed Q. Section 4 concludes the work.

2. Mathematical model and boundary conditions

The mathematical model is based on the two-dimensional conservation equations for mass, momentum and energy for an incompressible Newtonian fluid; for the buoyancy terms Boussinesq approximation is assumed. These equations have been supplemented by magnetohydrodynamic equations as derived from Maxwell equations [10] and modified suitably to facilitate numerical implementation [11]. It was found that for top and bottom heated walls the magnetohydrodynamic equations written in field components form, i.e. in (Bx, B_y) form do not satisfy the constraint of solenoidality of the magnetic field and hence the magnetic vector potential approach [4] was used.

The length, velocity, time and temperature scales used for nondimensionalization are H, k/H, H^2/k and ∇T, the temperature difference between the top and bottom walls. The magnetic field $B = (B_x, B_y)$ has been nondimensionalized using B_0, the strength of the vertically imposed uniform magnetic field. The equations in dimensionless nonconservative form can be cast as:

$$D = \nabla.V = 0 \tag{1}$$

$$\frac{Du}{Dt} = -\frac{\partial p}{\partial x} + Pr\nabla^2 u + \frac{Pr^2}{Pm} Q\left[B_y \left(\frac{\partial B_x}{\partial y} - \frac{\partial B_y}{\partial x} \right) \right] \tag{2}$$

$$\frac{Dv}{Dt} = -\frac{\partial p}{\partial y} + Pr\nabla^2 v + RaPrq + \frac{Pr^2}{Pm} Q\left[B_x \left(\frac{\partial B_y}{\partial x} - \frac{\partial B_x}{\partial y} \right) \right] \tag{3}$$

$$\frac{Dq}{Dt} = \nabla^2 q + \frac{Q}{Ra}\left(\frac{Pr^2}{Pm} \right) \frac{a\, gH}{C_p} (\nabla \times B)^2 \tag{4}$$

$$\frac{DB_x}{Dt} = B_x \frac{\partial u}{\partial x} + By \frac{\partial u}{\partial y} + \frac{Pr^2}{Pm} \nabla^2 B_x \tag{5}$$

$$\frac{DBy}{Dt} = B_x \frac{\partial v}{\partial x} + By \frac{\partial v}{\partial y} + \frac{Pr^2}{Pm} \nabla^2 B_y \tag{6}$$

$$D_m = \nabla.B = 0 \tag{7}$$

Equations (5) and (6) can be recast in vector potential approach using $\mathbf{B} = \nabla \times A$ where $\mathbf{A} = \mathrm{A}\ \mathbf{k}$

$$\frac{DA}{Dt} = \frac{Pr^2}{Pm} \nabla^2 \mathbf{A} \tag{8}$$

The Poisson equation for pressure is given as

$$\nabla^2 P = -\frac{\partial D}{\partial t} - 2\frac{\partial^2 uv}{\partial x \partial y} - \frac{\partial^2 u^2}{\partial x^2} - \frac{\partial^2 v^2}{\partial y^2} - u\frac{\partial D}{\partial x} - v\frac{\partial D}{\partial y}$$
$$+ Pr\nabla^2 D + RaPr\frac{\partial q}{\partial y} + \frac{Pr^2}{Pm}\left[Q\left(\frac{\partial C}{\partial x} + \frac{\partial D}{\partial y}\right)\right] \tag{9}$$
$$C = B_y\left(\frac{\partial B_x}{\partial y} - \frac{\partial B_y}{\partial x}\right)$$
$$D = B_x\left(\frac{\partial B_y}{\partial x} - \frac{\partial B_x}{\partial y}\right)$$

where ∇ is the Laplace operator, P, the dimensionless pressure, $V = (u, v)$, the dimensionless velocity field, q, the dimensionless temperature, D, the dilation of the incompressible flow field, D_m, the dilation of the magnetic field, and B_x and B_y are the horizontal and vertical dimensionless magnetic fields. The Rayleigh number is expressed as $Ra = agH^3\nabla T/vk$, where a is the thermal expansion coefficient, H, the depth of fluid layer, v, the kinematic viscosity, k, the thermal diffusivity, g, the acceleration due to gravity and ∇T, the temperature difference between the hot and cold walls; and $Q = sH^2{B_0}^2/r_0 v$, where s is the electrical conductivity of fluid, B_0, the imposed magnetic field, and r_0, the reference density. The Prandtl number is expressed as $Pr = v/k$ and the magnetic Prandtl number as $Pm = v/v_h$, where v_h is the magnetic viscosity. The second and third terms of eqns (2) and (3) are dimensionless Lorentz force components in x and y directions. The second term in eqn (4) is the Joule heating term which accounts for increase in internal energy brought about by induced currents. The viscous dissipation terms have been neglected in this study. The dilation D of the velocity field is explicitly satisfied in the pressure Poisson equation, while dilation D_m of the magnetic field is implicitly satisfied by the use of magnetic vector potential.

No-slip boundary conditions are enforced for the velocity components at all the walls. *è* is assumed to satisfy thermally conducting boundary conditions at the top and bottom walls, while Neumann boundary conditions $\partial q/\partial x = 0$ are assumed for the vertical side walls. All the rigid walls are assumed to be electrically insulated, hence the electric current density

$$j_z = \frac{\partial B_x}{\partial y} - \frac{\partial B_y}{\partial x} = 0$$

at all the walls. The top and bottom walls have a uniform vertically imposed magnetic field $B_y = B_0$.

The initial and boundary conditions are expressed as (Fig. 1)

$$t < 0\ ,\ u = v = 0,\ \grave{e} = 0,\ B_x = 0,\ B_y = 1$$

$$t >= 0,\ y = 0,\ 0 <= x <= 1,\ u = v = 0;\ \grave{e} = 1,\ B_y = 1,\ \frac{\partial B_x}{\partial y} = 0$$

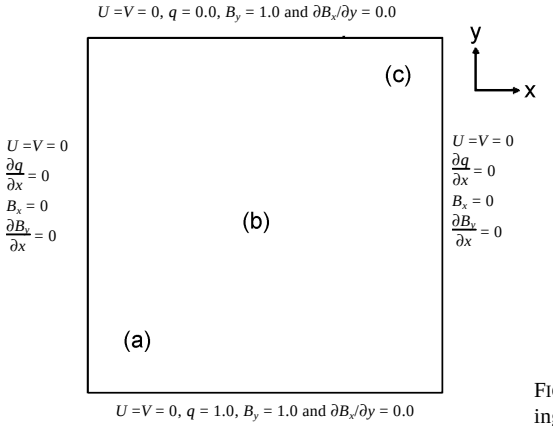

FIG. 1. Schematic view of the square enclosure showing boundary conditions and spatial location of points.

$$\text{at } y = 1,\ 0 <= x <= 1,\ u = v = 0;\ \dot{e} = 0,\ B_y = 1,\ \frac{\partial B_x}{\partial y} = 0$$

$$\text{at } x = 0,\ 0 < y < 1\ u = v = 0,\ \frac{\partial q}{\partial x} = 0\ ,\ B_x = 0,\ \frac{\partial B_y}{\partial x} = 0$$

$$\text{at } x = 1,\ 0 < y < 1\ u = v = 0,\ \frac{\partial q}{\partial x} = 0\ ,\ B_x = 0,\ \frac{\partial B_y}{\partial x} = 0.$$

The pressures on all the walls have been computed using the relevant momentum equations and cast as Dirichlet boundary conditions to get an unique solution of pressure in the interior.

The nonlinear convective terms in eqns (2)–(6) have been evaluated using two different second-order accurate upwind schemes, namely, (i) a variant of quadratic upstream interpolation for convection kinematics (QUICK) scheme as proposed by Leonard [12], and (ii) second-order upwind biased differencing (SOUBD) as implemented by Barton [13]. The diffusion terms are discretized using the three-point central differencing stencil, while time integration has been performed explicitly using Euler's first-order accurate scheme in order to capture the unsteady physics of the oscillatory flow regime. In order to satisfy the stability criterion of this explicit scheme, small time steps of the order of $5*10^{-8}$ have been used especially at higher *Ra* numbers.

The pressure Poisson equation (8) has been solved implicitly using strongly implicit procedure (SIP) as implemented by Ferziger and Peric [14] with L_2 norm tolerance limit of 10^{-9}. A collocated, nonuniform mesh of 51*51 ($(\Delta x)_{\min} = 0.002$, $(\Delta y)_{\min} = 0.002$) has been used for simulation with the location of the first grid point near the walls being made finer with increasing Rayleigh number. Since the variation between space-averaged Nusselt number (*Nu*) and the maximum *u* and *v* velocities was less than 2% for an 81*81 grid, all the simulations were performed, for computational effectiveness, using a 51*51 grid.

Table I
Comparison of different parameters of the present study with those of Ozoe and Maruo [5] at $Ra = 10^6$, $Q = 100$, $Pr = 0.054$, $Pm = 1$

Parameters	Present study	Reference [5]
$\varnothing$	0.21	0.206
Nu	1.010	1.004
B_x (max)	1.06	1.01
B_y (max)	0.92	0.957

Table II
Comparison of the present study with that of Hadjloucas *et al.* [7] at $Ra = 1.5*10^4$, $Q = 1600$, $Re_m = 1$, aspect ratio = 2

Ra	Q	$\varnothing$		Nu	
		Present study	Ref. [7]	Present study	Ref. [7]
$1.5*10^4$	40	231	226	1.47	1.48

3. Results and discussion

3.1. *Validation*

The numerical code developed has been validated by solving natural convection problem in differentially heated vertical sidewall cavity, with a vertically imposed uniform magnetic field and the results are compared with those of Hadjiloucas *et al.* [7], and Ozoe and Maruo [5]. Tables I and II show the comparison between the results of the present code and the earlier ones [5, 7]. Deviation of results for $\varnothing$ and Nu in both the cases is observed to be less than 2–3% on a nonuniform, collocated 51*51 mesh.

3.2. *Flow pattern analysis*

3.2.1. *Variation of Q at fixed Ra*

The computations were performed at fixed $Ra = 10^6$, while varying Q from a low value of 9 to a significantly high value of $9*10^4$. Figure 2 depicts the spatial evolution of rolls at the same instance of time for $Ra = 10^6$ at different values of Q. At $Q = 9$, the buoyancy forces dominate over the Lorentz forces and the flow field is oscillatory in time and space. The spatial evolution of rolls shows two incipient rolls cleaving into a multicellular flow pattern to be followed later by merging into a single roll. At $Q = 900$, the buoyancy and Lorentz forces are of the same order of magnitude, but as the buoyancy forces are still larger than Lorentz forces, the flow field retains its spatio-temporal oscillatory nature. The roll becomes symmetric at a later instance of time with no secondary eddies present. The generation of counter-vorticity by the Lorentz forces leads to the formation of complex vorticity structures. Further increase of $Q = 4900$ shows that Lorentz forces are comparable in strength to buoyancy forces and hence the oscillatory nature of the flow is dampened

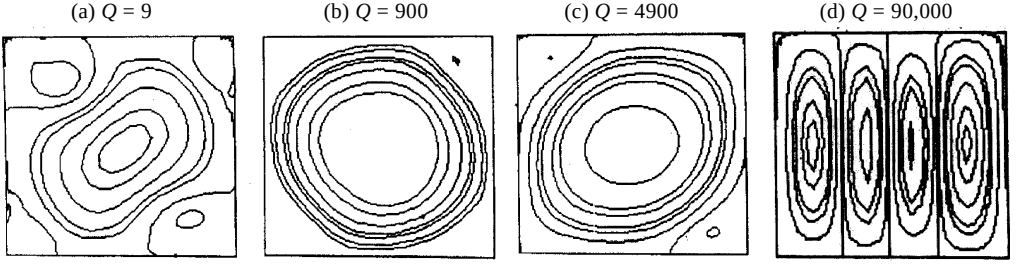

FIG. 2. Spatial evolution of rolls at the same instance of time for $Ra = 10^6$ at different Q values.

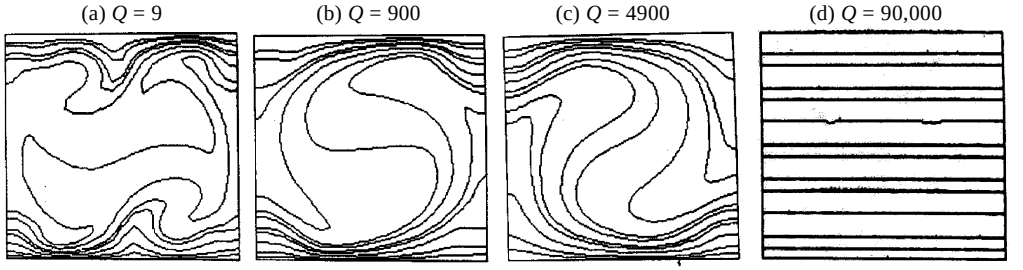

FIG. 3. Spatial evolution of isotherms at the same instance of time for $Ra = 10^6$ at different Q values.

leading to steady flow regime. The spatial variation of roll is akin to $Q = 900$ case, except that the higher amount of counter-vorticity generated by Lorentz forces leads to highly intermittent vorticity structures. Significant increase of Q to 90,000 leads to complete domination of Lorentz forces consequently resulting in total inhibition of convective flow. Moreover, as the rolls get elongated in the direction of the applied magnetic field, their horizontal wavelength reduces, generating a larger number of rolls.

Figure 3 depicts the spatial evolution of isotherms at the same instance of time for $Ra = 10^6$ at different values of Q. At $Q = 9$, the isotherms are characterized by incipience of thermal mushroom-shaped plumes rising from the bottom to be succeeded by rising and falling vertical drafts at the vertical side walls. Significant increase of Q to 90,000 leads to complete domination of Lorentz forces over buoyancy forces which results in straight isotherms throughout the enclosure. The flow can be considered to be dominated by conduction phenomenon as the convective motion has been totally inhibited.

Figure 4 depicts the magnetic lines of force at the same instance of time for $Ra = 10^6$ at different values of Q. At $Q = 9$, the magnetic lines of force change from left-right symmetric pattern to slightly asymmetric pattern with flux lines concentrating in regions of low convective velocities. At $Q = 900$, they have their left-right symmetry broken in the initial stages yielding to an oscillatory pattern of low-frequency periodicity. At $Q = 90{,}000$, the stationary and straight magnetic lines of force exhibit the phenomena of totally suppressed convection.

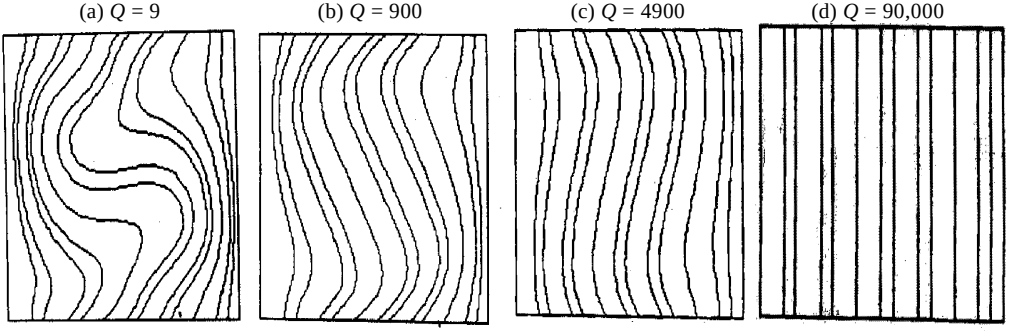

FIG. 4. Magnetic lines of force at the same instance of time for $Ra = 10^6$ and different Q values.

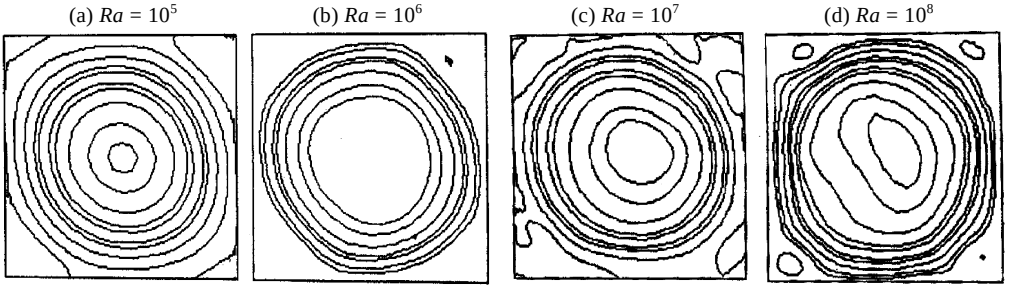

FIG. 5. Spatial evolution of rolls at the same instance of time for $Q = 900$ at different Ra values.

3.2.2. *Influence of Ra at fixed Q*

The computations were performed at $Q = 900$, while varying Ra from 10^5 to 10^8. Figure 5 depicts the evolution of rolls at the same instance of time for $Q = 900$ at different values of Ra. At $Ra = 10^5$, the Lorentz forces override the buoyancy force, resulting in a steady flow field in time and space. The spatial evolution of rolls for $Ra = 10^5$ shows that the two rolls merge after a significantly long time. The temporal variation of all the dynamical variables is steady. At $Ra = 10^6$, a large increase in the buoyancy forces overcomes the quadratic restoring Lorentz force, as is evident by the merging of the two symmetrical rolls during the initial stages of the flow development leading to the formation of single large rolls. Increase in Ra to 10^7 results in spatial evolution of rolls akin to that at $Ra = 10^6$. It is seen that the initial development is dominated by multicellular rolls which merge into a large spatially oscillating roll with secondary eddies at the corners of the enclosure. Further increase of Ra to 10^8 shows that buoyancy forces are the major contributors in the generation of a high-amplitude oscillatory flow field. In the incipient stages, a multicellular pattern of almost of equal strength, a counter-rotating roll is formed which merges to form a single large roll with wall constraints occupying a major portion of the enclosure. As the Ra is increased from 10^5 to 10^8, the shape of the rolls changes from circular to nearly square.

Figure 6 depicts the evolution of isotherms at the same instance of time for $Q = 900$ at different values of Ra. With increase in Ra from 10^5 to 10^8, the thermal boundary layers get thinner and thermal plumes rise from the bottom heated wall at initial stages. Also, the fluid rises and falls near the vertical walls, especially at higher Ra number.

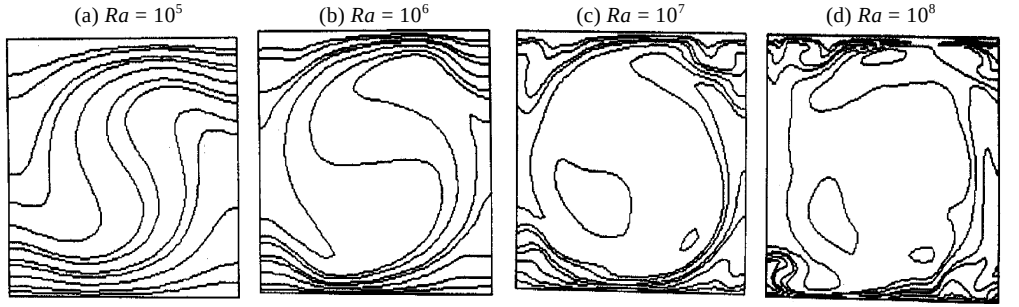

FIG. 6. Spatial evolution of isotherms at the same instance of time for $Q = 900$ at different Ra values.

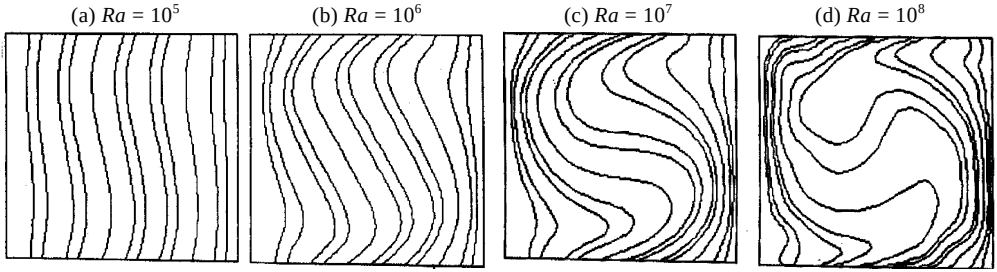

FIG. 7. Magnetic lines of force at the same instance of time for $Q = 900$ at different Ra values.

Figure 7 depicts the magnetic lines of force at the same instance of time for $Q = 900$ at different values of Ra. At $Ra = 10^5$, weak convective motion is suggested by low-frequency modulation of magnetic lines of force. At $Ra = 10^6$, the magnetic lines of force have their left-right symmetry and an oscillatory pattern of low-frequency periodicity. As Ra is increased to 10^8, these lines of force start concentrating in regions of low convective motion near the vertical walls. It is apparent that as the Ra number increases, the convective motion becomes more vigorous and the flux is being expelled from the kinematically active regions towards less-active zones near the vertical sidewalls.

3.3. *Heat transfer analysis*

3.3.1. *Increasing Q at fixed Ra*

On increase of Q from 9 to $9*10^4$ at a fixed $Ra = 10^6$, the magnitude of space-averaged Nu number decreases and oscillations get damped out (Fig. 8). The decrease in the magnitude of Nu can be correlated with Q at constant Ra to give power-law scaling of the form $Nu = C\,Q^{-0.072}$ where C = 10.78 (Fig. 9).

3.3.2. *Increasing Ra at fixed Q*

As the Ra is increased from 10^5 to 10^8 for a fixed $Q = 900$, it is seen that the space-averaged Nu number increases from steady value of 2.5 at $Ra = 10^5$ to a mean value of 10 at $Ra = 10^8$. This change is accompanied by the appearance of high-amplitude oscillations as the Ra number increases (Fig. 11). The increase in the magnitude of Nu can be correlated with

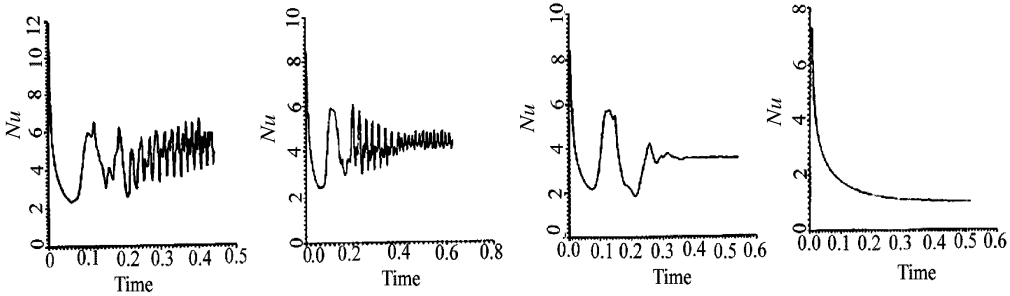

FIG. 8. Effect of increasing Q on Nu at fixed $Ra = 10^6$.

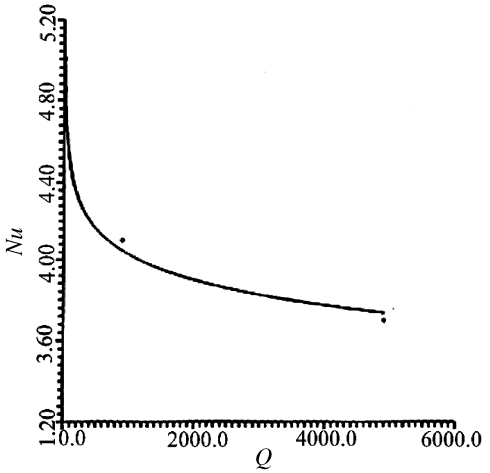

FIG. 9. Power-law scaling of Nu with Q for fixed $Ra = 10^6$.

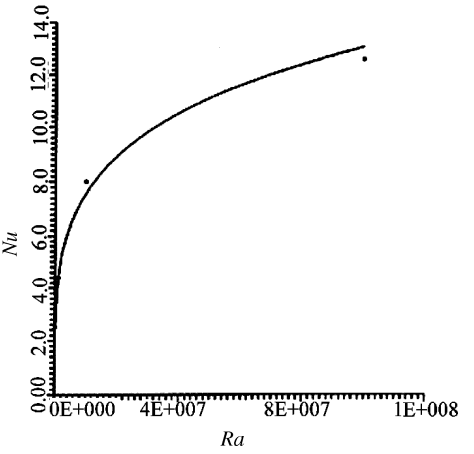

FIG. 11. Power-law scaling of Nu with Ra for fixed $Q = 900$.

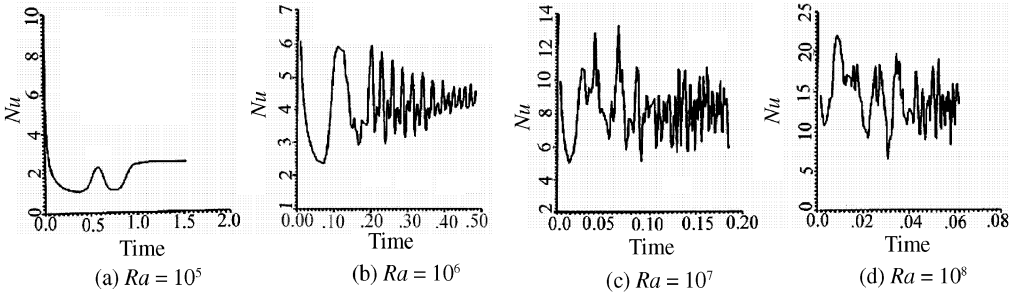

FIG. 10. Effect of increasing Ra on Nu at fixed $Q = 900$.

Ra at constant Q to give a power-law scaling (Fig. 10) of the form $Nu = D\ Ra^{0.21}$ where $D = 0.223$.

4. Conclusions

The spatio-temporal study yields oscillatory to steady fluid flow patterns on the increase of intensity of applied magnetic fields through variation of Q. It has been found that the strength of the magnetic field governs pattern formation as well as amplitudes of velocity for any particular Ra. The power spectrum confirms that with increase of Q the magnitude of the power content of the dominant frequencies decreases and the number of frequencies also reduces due to the removal of low-power frequencies.

With increase in Ra for a constant Q, the flow changes from steady to spatio-temporally oscillatory flow, with consequent increase in the magnitude of velocities. The power spectra show that power gets concentrated in a single dominant frequency as Ra is increased suggesting the appearance of two-dimensional turbulence with the characteristic feature of inverse cascade of energy.

References

1. J. Baumgartl, A. Hubert and G. Muller, The use of magnetohydrodynamic effects to investigate fluid flow in electrically conducting melts, *Phys. Fluids*, **A-5**, 3280–3289 (1993).
2. J. Baumgartl and G. Muller, Calculation of the effects of magnetic field damping on fluid flow: Comparison of magnetohydrodynamic models of different complexity, *Proc. Eighth European Symp. on Materials and Fluid Sciences in Microgravity*, Brussels, Belgium, pp. 161–164 (1992).
3. J. S. Walker, and B. F. Picologlou, Liquid metal flow in insulating rectangular expansion with a strong magnetic field, *J. Fluid Mech.*, **305**, 111–126 (1995).
4. N. O. Weiss, Convection in an imposed magnetic field. Part 1. The development of nonlinear convection, *J. Fluid Mech.*, **108**, 247–272 (1981).
5. H. Ozoe and E. Maruo, Magnetic and gravitational natural convection of melted silicon. Two-dimensional numerical computations for the rate of heat transfer, *JSME Int. J.*, **30**, 774–784 (1987).
6. H. Ozoe and K. Okada, The effect of the direction of the external magnetic field on the three-dimensional natural convection in a cubical enclosure, *Int. J. Heat Mass Transfer*, **32**, 1939–1954 (1989).
7. C. Hadjiloucas, H. Zhang and V. Prasad, Steady and oscillatory low Prandtl number convection in a vertical cavity: effects of magnetic field direction and aspect ratio, *ASME Proc. 32nd National Heat Transfer Conf.*, USA (1997).
8. S. Alchaar, P. Vasseur and E. Bilgen, Natural convection heat transfer in a rectangular enclosure with a transverse magnetic field, *ASME J. Heat Transfer*, **117**, 668–673 (1995).
9. A. Juel, T. Mullin, H. Ben Hadid and D. Henry, Magnetohydrodynamic convection in molten gallium, *J. Fluid Mech.*, **378**, 97–118 (1998).
10. P. H. Roberts, *An introduction to magnetohydrodynamics*, Longman (1967).
11. S. S. Sazhin and M. Makhlouf, Solutions of MHD problems based on a conventional computational fluid dynamics code, *Int. J. Numerical Meth. Fluids*, **21**, 433–442 (1995).
12. B. P. Leonard, A stable and accurate convective modelling procedure based on quadratic upstream interpolation, *Comp. Meth. Appl. Mech. Engng*, **19**, 59–98 (1979).
13. I. E. Barton, A numerical study of flow over a confined backward-facing step, *Int. J. Numerical Methods Fluids*, **21**, 653–665 (1995).
14. H. Ferziger and M. Peric, *Computational methods for fluid dynamics*, Springer Verlag (1996).